

Detection of the lensing galaxy in HE 2149–2745^{*}

Sebastian Lopez, Olaf Wucknitz, and Lutz Wisotzki

Hamburger Sternwarte, Universität Hamburg, Gojenbergsweg 112, 21029 Hamburg, Germany (slopez@hs.uni-hamburg.de)

Received; accepted

Abstract. We have obtained new *BVR*-band images of the gravitationally lensed QSO pair HE 2149–2745 A,B (QSO redshift $z_e = 2.033$; angular separation $\theta_{AB} = 1''.71$), under $1''$ seeing conditions. Subtraction of a scaled point-spread-function reveals an extended object of angular size comparable to θ_{AB} , and *R* magnitude of 20.4 lying between and equidistant to the QSOs. The geometry of the system leads us to interpret this object as the lensing agent responsible for the double QSO images. A fit to the galaxy surface brightness profile indicates an elliptical galaxy, which is further supported by the absence of Mg II in absorption. The lensing galaxy is not detected in *B* and *V*. We discuss possible lens models for this geometry constrained by our observations and consequences for the mass and redshift of the lens.

Key words: Quasars: individual: HE 2149–2745 – Quasars: general – Gravitational lensing

1. Introduction

Gravitational lensing of distant extragalactic sources (e.g., QSOs) by intervening large masses at low to moderate redshift (e.g., galaxies) has become a powerful tool of modern cosmology. The multiple images of lensed QSOs are expected to be separated by a few arc seconds in the sky, implying transverse line-of-sight (LOS) separations of up to few tens of kpc. The detection and study of the lensing agent provide an independent way to (i) probe the dark mass involved in the lensing potential (e.g., Natarajan et al. 1998); (ii) put constraints on the the Hubble parameter H_0 in case of QSO variability (Refsdal 1964). However, the position of the lensing agent, normally much fainter than the lensed source, is fairly difficult to determine. To date, about 20 lens redshifts have been determined out of twice as many known gravitational lens events.

In this letter we present new *BVR* images of the gravitationally lensed QSO pair HE 2149–2745 A,B aimed at

detecting the galaxy responsible for the double image. The QSO redshift is $z = 2.033$ and the angular separation between the QSO images is $\theta_{AB} = 1''.71$. As the QSO pair was discovered, the spectroscopic and *R*-band observations by Wisotzki et al. (1996) already revealed its lensing nature, but the detection of the lensing galaxy remained uncertain. Our new images confirm the presence of the lensing galaxy. The sampling is well below the small separation between the two QSO images, so an estimate of galaxy parameters is possible. They are discussed in the framework of possible lens scenarios.

2. Observations and image analysis

We observed HE 2149–2745 on August 8th, 1997, with SUSI on the 3.5m ESO NTT. SUSI uses a TEK CCD with 1024^2 $24 \mu\text{m}$ pixels corresponding to $0''.13$ in a $2'.2 \times 2'.2$ sky field of view. Despite a rather variable seeing several exposures could be taken under $\sim 1''$ seeing conditions. This was lucky given the bad weather conditions just days before the observations. The night was not photometric.

We obtained science exposures in the three bands *B* (5 exposures à 600 s), *V* (5 à 400 s), and *R* (9 à 300 s). We also obtained short exposures of the photometric standard star field PG2213-006 (Landolt 1992) to check for possible spatial variations of the point-spread function (PSF) and to normalize our magnitudes to the standard system. After bias-subtraction the images were corrected for detector pixel-to-pixel variations using combined twilight sky flat-fields. The effective width of a point source in the science frames, as measured for the only well-exposed star in the SUSI field (hereafter “star 3”; cf. Fig. 1 in Wisotzki et al. 1996), range from $1''.3$ to $1''.5$ in the *B*-band frames, from $1''.3$ to $1''.4$ (*V*), and from $1''.0$ to $1''.4$ (*R*). Due to this quality dispersion we decided to analyse each image *separately*.

All *BVR* exposures clearly resolve the QSO components (hereafter A and B, respectively). We used the DAOPHOT II package to derive the PSF and to obtain astrometric and photometric parameters in the frames containing the QSOs. The PSF was modeled with a $\beta = 2.5$ Moffat function whose parameters resulted from the fit to

Send offprint requests to: S. Lopez

^{*} Based on observations made at the European Southern Observatory, La Silla. Chile

star 3, allowing for empirical departures from the analytical form. A similar one-star fit and subsequent subtraction of the scaled PSF in the more crowded standard-star field demonstrated the spatial stability of the PSF shape, thus validating the use of just one star in its calculation.

3. Results

3.1. *R*-band images: the lensing galaxy

Fig. 1 (left) shows an *R*-band single exposure of HE 2149–2745 A,B with $\text{FWHM} = 1''.0$. The subtraction of the scaled PSF at the position of both QSO images clearly leaves a diffuse, ellipsoidal object lying between and more or less equidistant to A and B, as is shown in the right-hand panel. The simultaneous scaling of the PSF overfitted the fluxes at the A and B peaks, thus leaving small regions with relative negative residuals around both QSOs. This is expected given the contribution from the underlying object outside a few seeing radii; consequently, small corrections of roughly 0.01 (A) and 0.02 (B) magnitudes were made to recover the lacking flux. The mean flux values in the central region deviate 15σ from the background sky level. The stability of the PSF leads us to conclude that we have undoubtedly detected a galaxy in the LOSs to HE 2149–2745 A and B, most probably the gravitational lens.

Simple aperture photometry yields $R_G = 20.35 \pm 0.20$ for the galaxy. The error bar reflects the tolerance range allowed by the fine-tuning described in the above paragraph, and includes the zero-point uncertainty. For the sum of both QSO components we find $R_{A+B} = 16.30 \pm 0.04$. These magnitudes are based on the photometric results by Wisotzki et al. (1996) for star 3 (assuming it has not varied), and consider a color-term correction of 0.05 which reduces them to the Landolt (1992) system¹.

The relatively deep *R*-band images reveal many red non-stellar objects in the SUSI field of view, but no evident overdensity is observed close to the lensing galaxy to a limiting magnitude of $R \sim 23$. However, we cannot exclude the possibility that the galaxy belongs to a cluster since the small field of view implies transverse distances still compatible with cluster sizes. In particular, two of the objects, not much fainter than 20.4, lie within $12''$ of the galaxy position. It remains therefore unclear whether the galaxy belongs to a cluster or not.

Table 1 also gives the calibrated magnitudes of both QSO components. As the *V* magnitude of star 3 is not available we assumed $V - R = 0.46 \pm 0.06$ using a selected sample of stars with similar $B - R$ colors. We note that the magnitude difference between A and B is consistent with a flux ratio A to B of $f = 4.3$ for all three band filters.

Fig. 2 shows isophotal contours of the lensing galaxy. The isophotes are separated by 0.2 magnitudes, and the

¹ The *B* magnitude for star 3 given in Wisotzki et al. (1996) was erroneous and must be corrected to $B = 16.14$

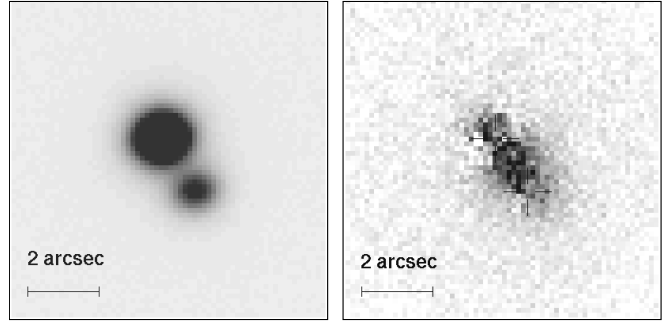


Fig. 1. *Left:* *R*-band 300 s exposure of HE 2149–2745 A,B. North is on the top, east to the right. *Right:* Same as in left-hand panel but after scaling and subtracting the PSF at the positions indicated with the crosses. Two exposures with similar effective seeing of $1''.0$ have been combined (600 s).

Table 1. Photometry and astrometry of HE 2149–2745 A,B and the lensing galaxy.

| | A | B | $m_A - m_B$ | Galaxy |
|----------|------------------|------------------|-----------------|------------------|
| <i>x</i> | 0.00 ± 0.03 | 0.90 ± 0.03 | | 0.50 ± 0.08 |
| <i>y</i> | 0.00 ± 0.03 | -1.45 ± 0.04 | | -0.73 ± 0.07 |
| <i>B</i> | 17.13 ± 0.03 | 18.70 ± 0.03 | 1.57 ± 0.04 | $\gtrsim 22.2^a$ |
| <i>V</i> | 16.82 ± 0.06 | 18.39 ± 0.06 | 1.57 ± 0.08 | $\gtrsim 21.7^a$ |
| <i>R</i> | 16.61 ± 0.02 | 18.20 ± 0.02 | 1.59 ± 0.03 | 20.35 ± 0.20 |

^a Approximate 3σ magnitude limits.

lowest contour level is approximately at 7σ above the background count. Note the distorted region near QSO A, probably due to photon-shot noise near the A peak (see below). The positions of A and B are marked with filled squares, since their errors are too small to appear at this scale. The angular separation between A and B is $\theta_{AB} = 1''.71 \pm 0''.07$, and the position angle is $\text{PA}_{AB} = 29.5^\circ \pm 1.0^\circ$. The position of the galaxy was derived using the isophotes at brighter levels than half the peak intensity: $x = 0''.50 \pm 0''.08$, and $y = -0''.73 \pm 0''.07$ relative to A. There is a small misalignment between this position and the QSO images, but alignment is possible within the measurement uncertainties. Its orientation coincides surprisingly well with the line joining A and B (\overline{AB}), with an ellipticity of $\epsilon \equiv (a - b)/(a + b) \sim 0.33$. The galaxy center lies nearly equidistant to both QSOs, with $\theta_{AG} = 0''.88$ and $\theta_{BG} = 0''.83$.

The good spatial sampling of our data allows an estimate of the galaxy parameters. A 180° section aligned with the south semimajor axis was used to fit isophotal ellipses to the flux values. Fig. 3 shows the averaged surface brightness profile (error bars). A de Vaucouleurs law and an exponential disk were fitted to the profile within $0''.5 \leq r \leq 1''.7$, thus including only values at the $> 3\sigma$

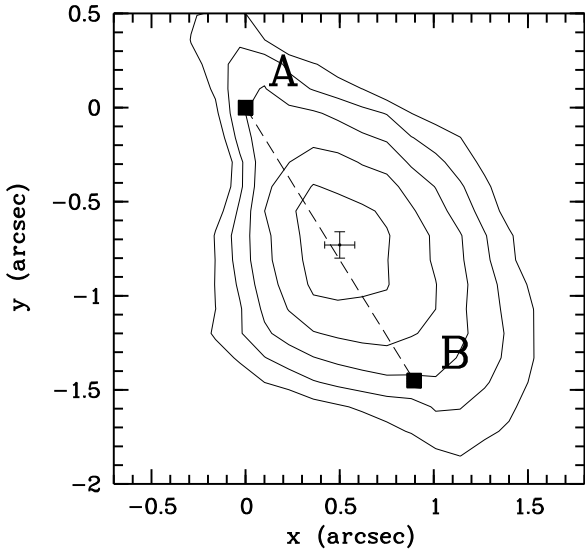


Fig. 2. Isophote contours of the lensing galaxy in intervals of 0.2 magnitudes. The lowest contour level is at 7σ above the sky background.

level but not significantly affected by the seeing smoothing. The final fit models result from re-constructing the isophotal ellipses with the fitted profiles and smoothing them with the PSF. We see that the data are better modeled by a $r^{1/4}$ law ($\chi^2_\nu = 0.3$) than by an exponential disk ($\chi^2_\nu = 2.2$), especially at the core. Furthermore, images taken under better seeing conditions should accentuate the concave shape of the observed profile. We take this result, though cautiously, as evidence for an elliptical galaxy.

3.2. *B* and *V* band images

The galaxy is not detected in the PSF-subtracted *B* and *V* band images. However, the region surrounding QSO image A is slightly overfitted at both sides of \overline{AB} . Such residuals are not observed for B. This “symmetric” overfit, though not significant ($\lesssim 2\sigma$ in *B* and only marginal in *V*), suggests A might be composed of two or more fainter point sources lying on \overline{AB} . We investigated this possibility (cf., Bade et al. 1997; Burud et al. 1998) in the *B*-band, as one expects here less contamination by a hypothetical foreground galaxy (in spite of the fact that the PSF is broader in the blue). However, attempts to re-fit A with two sources of nearly half its intensity failed at recovering the background level. It is difficult to establish on the basis of the present data what causes the low-quality fits in the *B* images. From an observational point of view, splitting of QSO image A in very close sub-components cannot be ruled out, but an underlying object could also contribute to slightly distort the QSO images. An explanation of this must await better quality data.

To put upper limits on the galaxy *B* and *V* brightness a variance frame was created which considers photon statis-

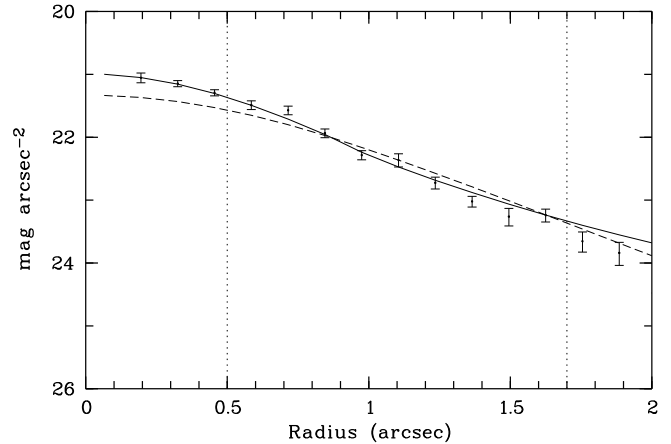


Fig. 3. Surface brightness profile of the lensing galaxy. *Solid line:* $r^{1/4}$ law fitted to the data within $0''.5 \leq r \leq 1''.7$, and convolved with the PSF. *Dashed line:* Same for an exponential disk. The fitting range is indicated by the vertical dotted lines.

tics (dominated by the QSO fluxes), readout noise, and the uncertainties introduced by background subtraction. Integration of the variances in a $3''.5$ radius aperture yields detection limits for *B* and *V*. In addition, we consider the fraction of possible galaxy light hidden in the QSO seeing disks and hence subtracted with the PSF. Analysis of *R* images with similar seeing as in *B* and *V* shows that this fraction can be as large as 0.7 (*B*) and 0.5 (*V*). The estimated (3σ) detection limits are listed in Table 1.

4. Discussion

4.1. Redshift of the galaxy

The redshift of the lensing galaxy can in principle be constrained by its color if we know its morphology. Besides the surface-profile fits, further evidence that we are observing an elliptical galaxy in front of HE 2149–2745 comes from the optical spectra of QSO A: no Mg II absorption system is detected down to an (observed) equivalent width limit of $\sim 0.3 \text{ \AA}$ (3σ). Given the small impact parameter ($\sim 7 h_{50}^{-1} \text{ kpc}$ at $z = 1$), this result almost excludes a disk-like galaxy in the foreground at $z > 0.35$.

The 3σ lower limit derived for the galaxy *V* magnitude (Table 1) puts a lower limit of $V - R \gtrsim 1.4$. This is the $V - R$ color an E galaxy would have at a redshift of ~ 0.3 or larger (using spectral energy distributions observed at $z = 0$ from Coleman, Wu & Weedman 1980). A bound consistent with this redshift is obtained from the $B - R$ color (Bressan, Chiosi & Fagotto 1994). The implied absolute luminosity for $z_G = 0.3$ is $M_R = -21.5$ (considering *K*-corrections, $H_0 = 50 \text{ km s}^{-1} \text{ Mpc}^{-1}$, and $q_0 = 0.5$), i.e., very close to M^* . An upper limit for z_G is difficult to establish, but for the observed R_G the expected luminosity beyond $z \sim 0.5$ becomes too large to be real. We thus arrive to $0.3 \lesssim z_G \lesssim 0.5$.

4.2. Lens models

Because of the symmetry of the mass distribution expected for any regular galaxy, the deflection angle and the amplification should be very similar for the two images of HE 2149–2745. This is also true if we include an external shear. To explain the flux ratio of 4.3, the dependence of the amplification on the positions has to be very strong. This can be achieved if the images are located near a critical curve, implying high amplifications.

Given the required sensitivity of the models for small changes of the positions and the small number of constraints, a maximum likelihood model fitting is not appropriate for this system; instead, we use an analytical approach to find the possible model parameters considering the measurement uncertainties.

We use a singular isothermal elliptical mass distribution (SIEMD) as given by Kassiola & Kovner (1993). As can be seen from Fig. 2, the images are almost exactly located on the major axis of the galaxy. To simplify the calculations, we use the line \overline{AB} as the major axis and project the center of the galaxy onto this line. We further include an external shear γ , whose source has to be located on the major or minor axis to be in agreement with the observed image positions. As observational parameters, we use the ratio of distances of the images from the center of the galaxy $f_x = \theta_{BG}/\theta_{AG}$ (nearly unity) and the amplification ratio $f = 4.3$. In addition, we force the two images to have different parity, which is a necessary condition to exclude the existence of more than two images. Even non-singular models (PIEMD) rule out the possible splitting of A in the radial direction.

On the main axis, the lens equation and the amplification for the SIEMD model with external shear read

$$x_s = (1 - \gamma)x - \alpha_0 \frac{1 - \epsilon^2}{2\sqrt{\epsilon}} \arctan \frac{2\sqrt{\epsilon}}{1 - \epsilon} \text{sign } x \quad ,$$

$$M_x^{-1} = (1 - \gamma) \left(1 + \gamma - \frac{\alpha_0(1 + \epsilon)}{|x|} \right) \quad .$$

Since a degeneracy in the models prevents the independent determination of ϵ and γ , we use the two above equations to define the parameter E ,

$$E \equiv \frac{1 + \gamma}{1 - \gamma} \frac{1 - \epsilon}{2\sqrt{\epsilon}} \arctan \frac{2\sqrt{\epsilon}}{1 - \epsilon} = \frac{(1 + f_x)(1 + ff_x)}{2f_x(1 + f)} \quad .$$

With our data, we get $E = 0.99 \pm 0.05$ (1σ). The uncertainty in E is dominated by the errors in the galaxy position. If the mass distribution has the same ellipticity as the light ($\epsilon = 0.33$), an external shear of $\gamma_{\min} = 0.21$ is needed to keep E inside the 1σ bounds. Because of the absence of very close galaxies or a rich cluster in the field, we do not expect such a large shear. For an ellipticity of $\epsilon = 0.2$, the minimal shear decreases to $\gamma_{\min} = 0.11$. Fig. 4 shows the possible parameters consistent with the measured positions and the flux ratio. Even for different parity of the images some very symmetrical models lead

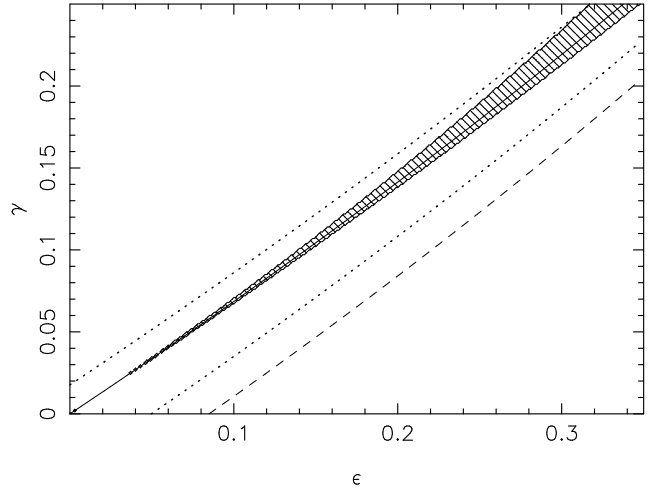


Fig. 4. Model parameters ϵ and γ consistent with the observations. Models with more than two images are shown hatched. The dotted lines are 1σ bounds of the measurements, the dashed line is a lower limit for γ independent of f_x . The solid line shows a symmetrical configuration with $f_x = 1$.

to more than two images (up to *eight* images are possible for SIEMD+shear models).

Only rough estimates for the absolute amplifications can be determined from the observations. For a best-fit model, we get $M_A \approx 70$. Considering the errors, a lower limit for $|M_A|$ of 27 (68% confidence) can be obtained.

To estimate the mass and velocity dispersion of the galaxy, we use a spherical model ($\epsilon = 0$). For lens redshifts of $z_d = 0.3$ (0.5), the mass inside the Einstein radius is $M = 1.5$ (2.4) $\times 10^{11} h_{50}^{-1} M_\odot$, and the velocity dispersion $\sigma_v = 205$ (230) km s^{-1} ($\Omega = 1$, $\lambda = 0$). The implied mass-to-light ratio is $M/L_R = 5$ (2) in solar units.

The expected order of magnitude for the time delay is about weeks. A better estimate must await more stringent constraints on the galaxy position. Given the geometry of the system, off-center spectroscopy of the galaxy should be possible from the ground under excellent seeing conditions, or with STIS onboard the *HST*.

Acknowledgements. We thank K. Jahnke for computing the surface brightness profile.

References

- Bade N., Siebert J., Lopez S., Voges W., Reimers D., 1997, *A&A* 317, L13
- Bressan A., Chiosi C., Fagotto F., 1994, *ApJS* 94, 63
- Burud I., Courbin F., Lidman C., et al., 1998, *ApJ* 501, L5
- Coleman G. D., Wu C., Weedman D. W., 1980, *ApJS* 43, 393
- Kassiola A., Kovner I., 1993, *ApJ* 417, 450
- Landolt A. U., 1992, *AJ* 104, 340
- Natarajan P., Kneib, J-P., Smail, I., Ellis, R. S., 1998, *ApJ* 499, 600
- Refsdal S., 1964, *MNRAS* 128, 295

Wisotzki L., Köhler T., Lopez S., Reimers D., 1996, A&A 315,
L405